Frontiers of Physics
https://doi.org/10.1007/s11467-021-1138-x
Front. Phys.
17(4), 42505 (2022)

RESEARCH ARTICLE

Nonreciprocal transition between two indirectly coupled energy levels

Xun-Wei Xu[1,2,†], **Hai-Quan Shi**[2], **Ai-Xi Chen**[2,3,‡]

[1] *Key Laboratory of Low-Dimensional Quantum Structures and Quantum Control of Ministry of Education, Key Laboratory for Matter Microstructure and Function of Hunan Province, Department of Physics and Synergetic Innovation Center for Quantum Effects and Applications, Hunan Normal University, Changsha 410081, China*
[2] *Department of Applied Physics, East China Jiaotong University, Nanchang 330013, China*
[3] *Department of Physics, Zhejiang Sci-Tech University, Hangzhou 310018, China*
Corresponding authors. E-mail: [†] *davidxu0816@163.com,* [‡] *aixichen@zstu.edu.cn*
Received November 16, 2021; accepted December 4, 2021

We propose a theoretical scheme to realize nonreciprocal transition between two energy levels that can not coupled directly. Suppose they are coupled indirectly by two auxiliary levels with a cyclic four-level configuration, and the four transitions in the cyclic configuration are controlled by external fields. The indirectly transition become nonreciprocal when the time reversal symmetry of the system is broken by the synthetic magnetic flux, i.e., the total phase of the external driving fields through the cyclic four-level configuration. The nonreciprocal transition can be identified by the elimination of a spectral line in the spontaneous emission spectrum. Our work introduces a feasible way to observe nonreciprocal transition in a wide range of multi-level systems, including natural atoms or ions with parity symmetry.

Keywords nonreciprocal transition, time reversal symmetry, synthetic magnetic flux, spontaneous emission spectrum

1 Introduction

Time reversal symmetry is the hypothesis that certain physical quantities are unchanged under time reversal transformation, which is related to reversibility of the system, such as the principle of detailed balancing in kinetic systems [1]. With the principle of detailed balance as a background, A. Einstein proposed his quantum theory of radiation [2] in 1916, which is now considered as the theoretical foundation of the laser, and one of the important corollaries is the absorption coefficient should be equal to the stimulated emission coefficient between two nondegenerate energy levels. However, sometimes we need to break the time reversal symmetry of atomic systems to yield fantastic phenomena, e.g., cyclic population transfer [3], controllable electromagnetically induced transparency [4], gain without inversion [5].

One important approach to break the time reversal symmetry of atomic systems is based on the cyclic three-level transitions in the chiral molecules [3, 6, 7], and in the superconducting qubit circuit with three Josephson junctions [8, 9]. The cyclic three-level transitions in multi-level atomic systems have been used to generate many interesting phenomena in single-photon level, including single-photon quantum routing [10], single-photon second-order nonlinear processes [11–13]. When the three possible transitions in the cyclic three-level configuration are driven by three mutually phase-locked driving fields, the time reversal symmetry of atomic system can be broken by the magnetic flux synthesized from the driving-field phase. In a recent experiment, time-reversal symmetry breaking and cyclic population transfer were revealed in a single nitrogen-vacancy spin system by controlling the global phase of the driving fields [14].

On the basis above, a multi-level atomic system with cyclic three-level configuration was proposed to realize significant difference between the stimulated emission and absorption coefficients of two nondegenerate energy levels [15], which was referred to as nonreciprocal transition. Different from the closed-contour spin dynamics [14], besides synthetic magnetism, reservoir engineering was also employed to eliminate one of the transitions in opposite directions [15]. Nonreciprocal transition in the multi-level atomic system provides us a new physical mechanism for designing nonreciprocal photon devices [16, 17] at single-photon level with single atoms [15]. Moreover, it was shown that the nonreciprocal transition can lead to the elimination of a spectral line in the spontaneous emission spectrum [18], which has a potential applica-

* arXiv: 2010.09604. This article can also be found at http://journal.hep.com.cn/fop/EN/10.1007/s11467-021-1138-x.

tion for the determination of enantiomeric excess of chiral molecules [18].

It is well known that due to the parity symmetry of the potential energy for usual natural atomic systems, described by $SO(3)$ or $SO(4)$, the parities of atomic eigenstates are well defined, and one-photon transitions between two energy levels require that the two corresponding eigenstates have opposite parities, which is referred to as the selection rule for the electric-dipole transitions. In a three-level atom system, at least two of the atomic eigenstates have the same parity and the one-photon dipole transition between them is forbidden. Thus, a cyclic three-level atom, i.e., the population cyclically transferred between three energy levels, cannot be realized with three one-photon transitions, except that the parity symmetry of the atomic system is broken. We note that the parity symmetry of a natural atom can be broken by applying a strong magnetic field [19, 20]. However, this technique is difficult to implement and is not commonly used.

In this paper, we propose a theoretical scheme to realize nonreciprocal transition between two energy levels that cannot coupled directly, which is significantly different from the models in Refs. [15, 18]. Most important, this provides a way to realize nonreciprocal transition without breaking the parity symmetry of the system, which open up a feasible way to observe nonreciprocal transition in wider systems, such as natural atoms or ions. Moreover, as two energy levels for nonreciprocal transition are not coupled directly, so there is not any strict restriction on the energy difference between them, and nonreciprocal transition can be realized between two degenerate energy levels, which goes beyond the limit of nondegenerate energy levels in Refs. [15, 18]. Our model can be used to design atom- or ion-mediated nonreciprocal devices with well-established technologies in the fields of cold atom [21] and ion trap [22, 23]. Such devices can find applications for quantum control of light in chiral quantum technologies [24] or topological photonics [25].

The remainder of this paper is organized as follows. In Section 2, a cyclic four-level configuration for two energy levels coupled indirectly by two auxiliary levels is introduced and the dynamical equations are given under the Weisskopf–Wigner approximation. The time evolution of the populations and the transition probabilities between the two energy levels are investigated, and nonreciprocal transitions are shown in Section 3. Moreover, the spontaneous emission spectra of the systems with nonreciprocal transitions are discussed in Section 4, which provide us a convenient way to measure nonreciprocal transitions in experiments. Finally, the conclusions is given in Section 5.

2 Hamiltonian and dynamical equations

We propose to realize nonreciprocal transition between two energy levels $|a\rangle$ and $|b\rangle$, under the assumption that they can not coupled directly. Suppose they are coupled indirectly through two auxiliary levels ($|c\rangle$ and $|d\rangle$) as a cyclic four-level configuration, and the four transitions are controlled by external fields with frequencies (ν_{ca}, ν_{cb}, ν_{db}, and ν_{da}), Rabi frequencies (Ω_{ca}, Ω_{cb}, Ω_{db}, and Ω_{da}) and phases (ϕ_{ca}, ϕ_{cb}, ϕ_{db}, and ϕ_{da}), as shown in Fig. 1. For different systems, the four (upper) levels may be coupled to the same lower level or to different lower levels respectively. Previous studies have shown that the spontaneous emission from multiple upper levels to the common lower level may result in spontaneous emission cancellation and spectral line elimination [26, 27], which is not the focus of this paper. In order to eliminate this effect, the spontaneous emission spectrum for the system will be derived for the case that the four upper levels are coupled to four different lower levels ($|g_a\rangle$, $|g_b\rangle$, $|g_c\rangle$, and $|g_d\rangle$) respectively with the same vacuum modes. The Hamiltonian is given by ($\hbar = 1$)

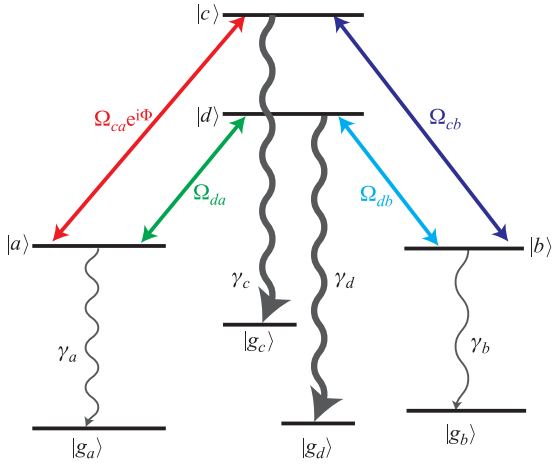

Fig. 1 Level diagram of an atom or ion with cyclic transitions for the four upper levels ($|a\rangle$, $|b\rangle$, $|c\rangle$, and $|d\rangle$), and they are coupled by the same vacuum modes to different lower levels ($|g_a\rangle$, $|g_b\rangle$, $|g_c\rangle$, and $|g_d\rangle$).

$$
\begin{aligned}
H = {} & \Omega_{ca} e^{i\phi_{ca}} e^{-i\Delta_{ca} t} |a\rangle\langle c| + \Omega_{cb} e^{i\phi_{cb}} e^{i\Delta_{cb} t} |c\rangle\langle b| \\
& + \Omega_{da} e^{i\phi_{da}} e^{i\Delta_{da} t} |d\rangle\langle a| + \Omega_{db} e^{i\phi_{db}} e^{-i\Delta_{db} t} |b\rangle\langle d| \\
& + \sum_k \Big[g_k^a e^{i(\omega_{ag} - \omega_k)t} v_k |a\rangle\langle g_a| \\
& + g_k^b e^{i(\omega_{bg} - \omega_k)t} v_k |b\rangle\langle g_b| \Big] \\
& + \sum_k \Big[g_k^c e^{i(\omega_{cg} - \omega_k)t} v_k |c\rangle\langle g_c| \\
& + g_k^d e^{i(\omega_{dg} - \omega_k)t} v_k |d\rangle\langle g_d| \Big] \\
& + \text{H.c.}, \qquad (1)
\end{aligned}
$$

where v_k and $v_k^\dagger$ are annihilation and creation operators for photons in the kth vacuum mode with frequency ω_k (k denotes both the momentum and polarization of the

vacuum modes); ω_{ij} and ω_{ig} are the frequency differences between levels $|i\rangle$ and $|j\rangle$, and between $|i\rangle$ and $|g_i\rangle$ respectively, with $(i,j=a,b,c,d)$; $\Delta_{ij}\equiv\omega_{ij}-\nu_{ij}$ is the detuning between the atomic transition $|i\rangle\leftrightarrow|j\rangle$ and the driving field, and g_k^i is the coupling strength between the atomic transition $|i\rangle\leftrightarrow|g_i\rangle$ and the kth vacuum mode. With the replacement $|b\rangle\rightarrow \mathrm{e}^{\mathrm{i}\phi_{cb}}|b\rangle$, $|d\rangle\rightarrow \mathrm{e}^{\mathrm{i}(\phi_{db}+\phi_{cb})}|d\rangle$, $|a\rangle\rightarrow \mathrm{e}^{\mathrm{i}(\phi_{da}+\phi_{db}+\phi_{cb})}|a\rangle$, $g_k^b\rightarrow g_k^b\mathrm{e}^{-\mathrm{i}\phi_{cb}}$, $g_k^d\rightarrow g_k^d\mathrm{e}^{-\mathrm{i}(\phi_{db}+\phi_{cb})}$, and $g_k^a\rightarrow g_k^a\mathrm{e}^{-\mathrm{i}(\phi_{da}+\phi_{db}+\phi_{cb})}$, the Hamiltonian is rewritten as

$$\begin{aligned}H=&\,\Omega_{ca}\mathrm{e}^{\mathrm{i}\Phi}\mathrm{e}^{-\mathrm{i}\Delta_{ca}t}|a\rangle\langle c|+\Omega_{cb}\mathrm{e}^{\mathrm{i}\Delta_{cb}t}|c\rangle\langle b|\\&+\Omega_{da}\mathrm{e}^{\mathrm{i}\Delta_{da}t}|d\rangle\langle a|+\Omega_{db}\mathrm{e}^{-\mathrm{i}\Delta_{db}t}|b\rangle\langle d|\\&+\sum_k\Big[g_k^a\mathrm{e}^{\mathrm{i}(\omega_{ag}-\omega_k)t}v_k|a\rangle\langle g_a|\\&+g_k^b\mathrm{e}^{\mathrm{i}(\omega_{bg}-\omega_k)t}v_k|b\rangle\langle g_b|\Big]\\&+\sum_k\Big[g_k^c\mathrm{e}^{\mathrm{i}(\omega_{cg}-\omega_k)t}v_k|c\rangle\langle g_c|\\&+g_k^d\mathrm{e}^{\mathrm{i}(\omega_{dg}-\omega_k)t}v_k|d\rangle\langle g_d|\Big]\\&+\mathrm{H.c.},\end{aligned}\tag{2}$$

where $\Phi\equiv\phi_{ca}+\phi_{db}+\phi_{cb}+\phi_{da}$ is the total phase of the four strong driving fields through the cycle-transition $|a\rangle\rightarrow|d\rangle\rightarrow|b\rangle\rightarrow|c\rangle\rightarrow|a\rangle$, i.e., the synthetic magnetic flux. Moreover, real coupling strength g_k^i is assumed for the phase of g_k^i does not matter in the following discussions. For simplicity, we also make the assumption of resonance $\Delta_c\equiv\Delta_{ac}=\Delta_{bc}$ and $\Delta_d\equiv\Delta_{da}=\Delta_{db}$.

In the following, we will discuss the indirect transition between levels $|a\rangle$ and $|b\rangle$ based on the Schrödinger equation under the Weisskopf–Wigner approximation [28, 29]. We assume that the system is prepared in level $|a\rangle$ or $|b\rangle$ initially, i.e., $|\psi(0)\rangle=|a\rangle|0\rangle$ or $|\psi(0)\rangle=|b\rangle|0\rangle$ with $|0\rangle$ denoting the vacuum state. According to the Schrödinger equation, $\mathrm{d}|\psi(t)\rangle/\mathrm{d}t=-\mathrm{i}H|\psi(t)\rangle$, the state vector at time t can be written as

$$\begin{aligned}|\psi(t)\rangle=&\,[A(t)|a\rangle+B(t)|b\rangle+C(t)|c\rangle+D(t)|d\rangle]|0\rangle\\&+\sum_{i=a,b,c,d}\sum_k G_k^i(t)v_k^\dagger|g_i\rangle|0\rangle,\end{aligned}\tag{3}$$

with occupation populations $|A(t)|^2$, $|B(t)|^2$, $|C(t)|^2$, $|D(t)|^2$, and $|G_k^i(t)|^2$ in the corresponding levels. Under the Weisskopf–Wigner approximation [28, 29], the dynamical behaviors for the coefficients are obtained as

$$\begin{aligned}\frac{\mathrm{d}}{\mathrm{d}t}A(t)=&-\frac{\gamma_a}{2}A(t)-\mathrm{i}\Omega_{ca}\mathrm{e}^{\mathrm{i}\Phi}\mathrm{e}^{-\mathrm{i}\Delta_c t}C(t)\\&-\mathrm{i}\Omega_{da}\mathrm{e}^{-\mathrm{i}\Delta_d t}D(t),\end{aligned}\tag{4}$$

$$\begin{aligned}\frac{\mathrm{d}}{\mathrm{d}t}B(t)=&-\frac{\gamma_b}{2}B(t)-\mathrm{i}\Omega_{cb}\mathrm{e}^{-\mathrm{i}\Delta_c t}C(t)\\&-\mathrm{i}\Omega_{db}\mathrm{e}^{-\mathrm{i}\Delta_d t}D(t),\end{aligned}\tag{5}$$

$$\begin{aligned}\frac{\mathrm{d}}{\mathrm{d}t}C(t)=&-\frac{\gamma_c}{2}C(t)-\mathrm{i}\Omega_{ca}\mathrm{e}^{-\mathrm{i}\Phi}\mathrm{e}^{\mathrm{i}\Delta_c t}A(t)\\&-\mathrm{i}\Omega_{cb}\mathrm{e}^{\mathrm{i}\Delta_c t}B(t),\end{aligned}\tag{6}$$

$$\begin{aligned}\frac{\mathrm{d}}{\mathrm{d}t}D(t)=&-\frac{\gamma_d}{2}D(t)-\mathrm{i}\Omega_{da}\mathrm{e}^{\mathrm{i}\Delta_d t}A(t)\\&-\mathrm{i}\Omega_{db}\mathrm{e}^{\mathrm{i}\Delta_d t}B(t),\end{aligned}\tag{7}$$

$$\frac{\mathrm{d}}{\mathrm{d}t}G_k^a(t)=-\mathrm{i}g_k^a\mathrm{e}^{-\mathrm{i}(\omega_{ag}-\omega_k)t}A(t),\tag{8}$$

$$\frac{\mathrm{d}}{\mathrm{d}t}G_k^b(t)=-\mathrm{i}g_k^b\mathrm{e}^{-\mathrm{i}(\omega_{bg}-\omega_k)t}B(t),\tag{9}$$

$$\frac{\mathrm{d}}{\mathrm{d}t}G_k^c(t)=-\mathrm{i}g_k^c\mathrm{e}^{-\mathrm{i}(\omega_{cg}-\omega_k)t}C(t),\tag{10}$$

$$\frac{\mathrm{d}}{\mathrm{d}t}G_k^d(t)=-\mathrm{i}g_k^d\mathrm{e}^{-\mathrm{i}(\omega_{dg}-\omega_k)t}D(t),\tag{11}$$

with the decay rates $\gamma_a=2\pi(g_k^a)^2\rho(\omega_{ag})$, $\gamma_b=2\pi(g_k^b)^2\rho(\omega_{bg})$, $\gamma_c=2\pi(g_k^c)^2\rho(\omega_{cg})$, and $\gamma_d=2\pi(g_k^d)^2\rho(\omega_{dg})$, and mode density $\rho(\omega_k)$. The dynamical equations (4)–(7) can be rewritten with constant coefficients as

$$\frac{\mathrm{d}}{\mathrm{d}t}A(t)=-\frac{\gamma_a}{2}A(t)-\mathrm{i}\Omega_{ca}\mathrm{e}^{\mathrm{i}\Phi}\widetilde{C}(t)-\mathrm{i}\Omega_{da}\widetilde{D}(t),\tag{12}$$

$$\frac{\mathrm{d}}{\mathrm{d}t}B(t)=-\frac{\gamma_b}{2}B(t)-\mathrm{i}\Omega_{cb}\widetilde{C}(t)-\mathrm{i}\Omega_{db}\widetilde{D}(t),\tag{13}$$

$$\begin{aligned}\frac{\mathrm{d}}{\mathrm{d}t}\widetilde{C}(t)=&\left(-\mathrm{i}\Delta_c-\frac{\gamma_c}{2}\right)\widetilde{C}(t)-\mathrm{i}\Omega_{ca}\mathrm{e}^{-\mathrm{i}\Phi}A(t)\\&-\mathrm{i}\Omega_{cb}B(t),\end{aligned}\tag{14}$$

$$\begin{aligned}\frac{\mathrm{d}}{\mathrm{d}t}\widetilde{D}(t)=&\left(-\mathrm{i}\Delta_d-\frac{\gamma_d}{2}\right)\widetilde{D}(t)-\mathrm{i}\Omega_{da}A(t)\\&-\mathrm{i}\Omega_{db}B(t),\end{aligned}\tag{15}$$

with the definitions $\widetilde{C}(t)\equiv\mathrm{e}^{-\mathrm{i}\Delta_c t}C(t)$, $\widetilde{D}(t)\equiv\mathrm{e}^{-\mathrm{i}\Delta_d t}D(t)$. It is worth mentioning that, here we have ignored the effects of the spontaneous decay between the four upper excited states, based on the assumption that the spontaneous relaxation between the four upper excited states is much slower than the spontaneous decay from the excited states to the ground states [30], and also much slower than the coherent transition between the excited states induced by the strong driving fields.

3 Transition probabilities

To gain insight into the transition probabilities between energy levels $|a\rangle$ and $|b\rangle$, we will solve the dynamic equations (12)–(15) both analytically and numerically. The dynamic equations (12)–(15) can be rewritten as an effective Schrödinger equation

$$\mathrm{i}\frac{\mathrm{d}\Psi(t)}{\mathrm{d}t}=H_{\mathrm{eff}}\Psi(t),\tag{16}$$

with state vector $\Psi(t)=\left[A(t),B(t),\widetilde{C}(t),\widetilde{D}(t)\right]^{\mathsf{T}}$, and effective Hamiltonian as

$$H_{\text{eff}}=\begin{pmatrix} -\mathrm{i}\frac{\gamma_a}{2} & 0 & \Omega_{ca}\mathrm{e}^{\mathrm{i}\Phi} & \Omega_{da} \\ 0 & -\mathrm{i}\frac{\gamma_b}{2} & \Omega_{cb} & \Omega_{db} \\ \Omega_{ca}\mathrm{e}^{-\mathrm{i}\Phi} & \Omega_{cb} & \Delta_c-\mathrm{i}\frac{\gamma_c}{2} & 0 \\ \Omega_{da} & \Omega_{db} & 0 & \Delta_d-\mathrm{i}\frac{\gamma_d}{2} \end{pmatrix}. \tag{17}$$

The formal solutions for Eq. (16) can be written as

$$\Psi(t)=U(t)\Psi(0), \tag{18}$$

with initial vector $\Psi(0)=[A(0),B(0),C(0),D(0)]^{\mathsf{T}}$, and time-evolution matrix

$$U(t)\equiv\mathrm{e}^{-\mathrm{i}H_{\text{eff}}t}. \tag{19}$$

The transition probabilities $T_{ba}(t)$ for $|a\rangle\rightarrow|b\rangle$ and $T_{ab}(t)$ for $|b\rangle\rightarrow|a\rangle$ can be defined from the time-evolution matrix $U(t)$ as

$$T_{ba}(t)\equiv|U_{21}(t)|^2, \tag{20}$$

$$T_{ab}(t)\equiv|U_{12}(t)|^2, \tag{21}$$

where the subscripts 1 and 2 are the row and column numbers of the matrix $U(t)$. Moreover, the isolation for the nonreciprocal transition between levels $|a\rangle$ and $|b\rangle$ is defined by

$$I(t)\equiv\frac{T_{ab}(t)}{T_{ba}(t)}. \tag{22}$$

Under the assumption that the decay rates of the upper levels $|c\rangle$ and $|d\rangle$ are much larger than the other parameters, i.e., $\min\{\gamma_c,\gamma_d\}\gg\max\{\gamma_a,\gamma_b,\Omega_{ca},\Omega_{cb},\Omega_{da},\Omega_{db}\}$, we can eliminate the auxiliary levels $|c\rangle$ and $|d\rangle$ adiabatically. By setting $d\widetilde{C}(t)/dt=d\widetilde{D}(t)/dt=0$ in Eqs. (14) and (15), we obtain

$$\widetilde{C}(t)=-\frac{\mathrm{i}\Omega_{ca}}{\mathrm{i}\Delta_c+\frac{\gamma_c}{2}}\mathrm{e}^{-\mathrm{i}\Phi}A(t)-\frac{\mathrm{i}\Omega_{cb}}{\mathrm{i}\Delta_c+\frac{\gamma_c}{2}}B(t), \tag{23}$$

$$\widetilde{D}(t)=\frac{-\mathrm{i}\Omega_{da}}{\mathrm{i}\Delta_d+\frac{\gamma_d}{2}}A(t)+\frac{-\mathrm{i}\Omega_{db}}{\mathrm{i}\Delta_d+\frac{\gamma_d}{2}}B(t). \tag{24}$$

Substitute these into Eqs. (12) and (13), the effective dynamic equations for levels $|a\rangle$ and $|b\rangle$ can be written as

$$\frac{\mathrm{d}}{\mathrm{d}t}A(t)=-\left(\frac{\gamma_{a,\text{eff}}}{2}+\mathrm{i}\Delta_{a,\text{eff}}\right)A(t)-J_{ab}B(t), \tag{25}$$

$$\frac{\mathrm{d}}{\mathrm{d}t}B(t)=-\left(\frac{\gamma_{b,\text{eff}}}{2}+\mathrm{i}\Delta_{b,\text{eff}}\right)B(t)-J_{ba}A(t) \tag{26}$$

with effective decay rates

$$\gamma_{a,\text{eff}}=\gamma_a+\frac{4\gamma_c\Omega_{ca}^2}{4\Delta_c^2+\gamma_c^2}+\frac{4\gamma_d\Omega_{da}^2}{4\Delta_d^2+\gamma_d^2}, \tag{27}$$

$$\gamma_{b,\text{eff}}=\gamma_b+\frac{4\gamma_c\Omega_{cb}^2}{4\Delta_c^2+\gamma_c^2}+\frac{4\gamma_d\Omega_{db}^2}{4\Delta_d^2+\gamma_d^2}, \tag{28}$$

effective detunings

$$\Delta_{a,\text{eff}}=-\frac{4\Delta_c\Omega_{ca}^2}{4\Delta_c^2+\gamma_c^2}-\frac{4\Delta_d\Omega_{da}^2}{4\Delta_d^2+\gamma_d^2}, \tag{29}$$

$$\Delta_{b,\text{eff}}=-\frac{4\Delta_c\Omega_{cb}^2}{4\Delta_c^2+\gamma_c^2}-\frac{4\Delta_d\Omega_{db}^2}{4\Delta_d^2+\gamma_d^2}, \tag{30}$$

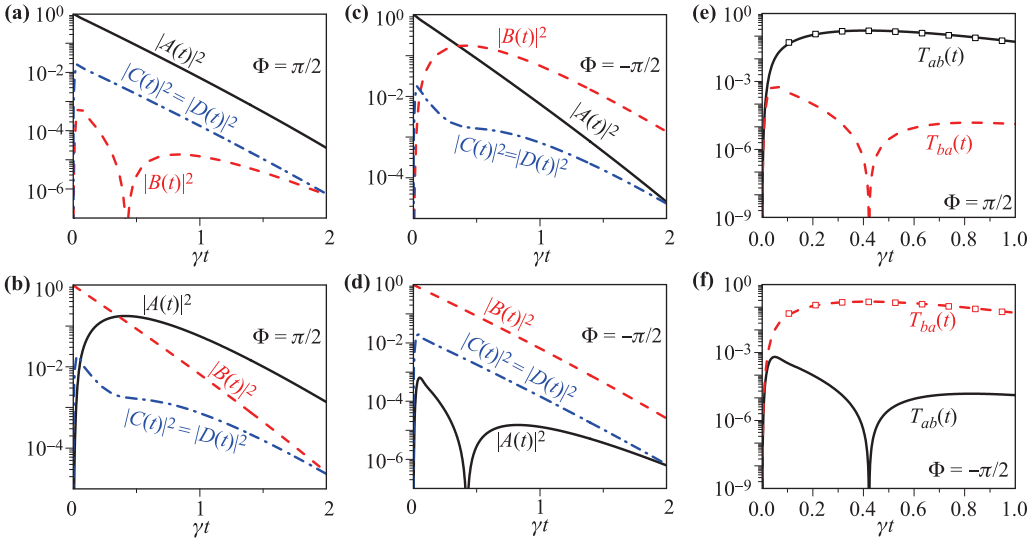

Fig. 2 The populations $|A(t)|^2$ (black solid curve), $|B(t)|^2$ (red dashed curve), and $|C(t)|^2=|D(t)|^2$ (blue dashed-dot curve) are plotted as functions of the time γt for: $\Phi=\pi/2$ in **(a)** and **(b)**; $\Phi=-\pi/2$ in **(c)** and **(d)**. The initial conditions are $A(0)=1$ and $B(0)=C(0)=D(0)=0$ for (a) and (c), $B(0)=1$ and $A(0)=C(0)=D(0)=0$ for (b) and (d). The transition probabilities $T_{ab}(t)$ (black solid curve) and $T_{ba}(t)$ (red dashed curve) are plotted as functions of the time γt for: **(e)** $\Phi=\pi/2$; **(f)** $\Phi=-\pi/2$. The other parameters are $\gamma_a=\gamma_b=\gamma$, $\gamma_c=\gamma_d=100\gamma$, $\Omega_{ca}=\Omega_{cb}=\Omega_{da}=\Omega_{db}=10\gamma$, $\Delta_c=-\Delta_d=50\gamma$.

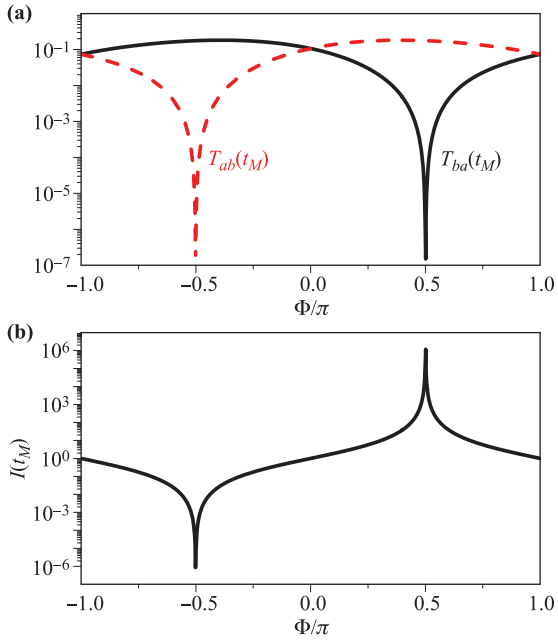

Fig. 3 **(a)** The transition probabilities $T_{ba}(t)$ and $T_{ab}(t)$, and **(b)** the isolation $I(t)$ are plotted as functions of the synthetic magnetic flux Φ at time $t = t_M$. The other parameters are the same as in Fig. 2.

and effective coupling coefficients

$$J_{ab} = \frac{\Omega_{ca}\Omega_{cb}e^{i\Phi}}{i\Delta_c + \frac{\gamma_c}{2}} + \frac{\Omega_{da}\Omega_{db}}{i\Delta_d + \frac{\gamma_d}{2}}, \tag{31}$$

$$J_{ba} = \frac{\Omega_{ca}\Omega_{cb}e^{-i\Phi}}{i\Delta_c + \frac{\gamma_c}{2}} + \frac{\Omega_{da}\Omega_{db}}{i\Delta_d + \frac{\gamma_d}{2}}. \tag{32}$$

The condition for nonreciprocal transition is $J_{ab} \neq J_{ba}$, i.e., $\Phi \neq n\pi$ (n is an integer). This can be understood intuitively that $\Phi \neq n\pi$ breaks the time-reversal symmetry of the Hamiltonian given in Eq. (2).

One necessary condition for optimal nonreciprocal transition is one of the effective coupling coefficients (J_{ab} or J_{ba}) equal zero, i.e.,

$$e^{\pm i\Phi} = -\frac{(i2\Delta_c + \gamma_c)}{(i2\Delta_d + \gamma_d)}\frac{\Omega_{da}\Omega_{db}}{\Omega_{ca}\Omega_{cb}}. \tag{33}$$

The transition probabilities from $|a\rangle$ to $|b\rangle$ [$T_{ba}(t)$] and from $|b\rangle$ to $|a\rangle$ [$T_{ab}(t)$] can be obtained approximately under this condition. For simplicity, we choose the symmetric parameters: $\Omega_{ca} = \Omega_{cb} = \Omega_{da} = \Omega_{db}$, $\gamma_a = \gamma_b$, $\gamma_c = \gamma_d$, $\Delta_c = -\Delta_d$. The condition $J_{ab} = 0$ ($J_{ba} = 0$) is satisfied for $\Phi = -\pi/2$ ($\Phi = \pi/2$) with detuning $\Delta_c = -\Delta_d = \gamma_c/2 = \gamma_d/2$, and we have transition probabilities

$$T_{ba}(t) \approx \left| J_{ba} t \exp\left[-\left(\frac{\gamma_{b,\mathrm{eff}}}{2} + i\Delta_{b,\mathrm{eff}} \right) t \right] \right|^2, \tag{34}$$

for initial conditions $A(0) = 1$ and $B(0) = C(0) = D(0) = 0$, and

$$T_{ab}(t) \approx \left| J_{ab} t \exp\left[-\left(\frac{\gamma_{a,\mathrm{eff}}}{2} + i\Delta_{a,\mathrm{eff}} \right) t \right] \right|^2 \tag{35}$$

for initial conditions $B(0) = 1$ and $A(0) = C(0) = D(0) = 0$. The transition probabilities are time dependent, and the time for maximal transition probability is

$$t_M \approx \frac{2}{\gamma_{b,\mathrm{eff}}} = \frac{2}{\gamma_{a,\mathrm{eff}}}, \tag{36}$$

with transition probabilities

$$T_{ba}(t_M) \approx \left| \frac{2}{e}\frac{J_{ba}}{\gamma_{b,\mathrm{eff}}} \right|^2, \tag{37}$$

$$T_{ab}(t_M) \approx \left| \frac{2}{e}\frac{J_{ab}}{\gamma_{a,\mathrm{eff}}} \right|^2, \tag{38}$$

where e is the mathematical constant approximately equal to 2.71828.

The populations $|A(t)|^2$ (black solid curve), $|B(t)|^2$ (red dashed curve), and $|C(t)|^2 = |D(t)|^2$ (blue dashed-dot curve) obtained from Eqs. (17)–(19) are plotted as functions of the time t in Figs. 2(a)–(d). It is clear that the population can transfer from the level $|b\rangle$ to level $|a\rangle$ for $\Phi = \pi/2$, but almost no population will transfer from the level $|a\rangle$ to level $|b\rangle$. In contrast, the population can transfer from the level $|a\rangle$ to level $|b\rangle$, but almost no population will transfer from the level $|b\rangle$ to level $|a\rangle$ when $\Phi = -\pi/2$.

The transition probabilities from $|b\rangle$ to $|a\rangle$ [$T_{ab}(t)$] and from $|a\rangle$ to $|b\rangle$ [$T_{ba}(t)$] can also be obtained from Eqs. (19)–(21). They are plotted as functions of time t in Figs. 2(e) and (f). It is clear that $T_{ab}(t) \gg T_{ba}(t)$ for $\phi = \pi/2$, and $T_{ab}(t) \ll T_{ba}(t)$ for $\phi = -\pi/2$, i.e., the transitions between levels $|b\rangle$ and $|a\rangle$ are nonreciprocal. The approximate analytical results given in Eqs. (34) and (35) are shown by open squares in Figs. 2(e) and (f), which agree well with the solid and dashed curves obtained from Eqs. (19)–(21).

Furthermore, the dependence of the transition probabilities $T_{ba}(t)$ and $T_{ab}(t)$ on the synthetic magnetic flux Φ is show in Fig. 3(a). At time $t = t_M$, we have $T_{ba}(t) < T_{ab}(t)$ for synthetic magnetic flux $0 < \Phi < \pi$; in the contrast, we have $T_{ba}(t) > T_{ab}(t)$ for synthetic magnetic flux $-\pi < \Phi < 0$. As shown in Fig. 3(b), under the conditions $\Omega_{ca} = \Omega_{cb} = \Omega_{da} = \Omega_{db}$ and $\Delta_c = -\Delta_d = \gamma_c/2 = \gamma_d/2$, the optimal isolation $I(t)$ is obtained with synthetic magnetic flux $\Phi = \pm\pi/2$.

4 Spontaneous emission spectrum

In this section, we will show that the nonreciprocal transitions can be identified by measuring the spontaneous

emission spectra of the system. The spontaneous emission spectra of the system can be derived analytically by the Laplace transform method [26, 27]. Taking the Laplace transform, i.e., $\overline{O}(s)=\int_0^{+\infty}O(t)\,\mathrm{e}^{-st}\mathrm{d}t$, the solution of the effective Schrödinger equation (16), $\overline{\Psi}(s)=\left[\overline{A}(s),\overline{B}(s),\overline{\widetilde{C}}(s),\overline{\widetilde{D}}(s)\right]^{\mathrm{T}}$, is given by

$$\overline{\Psi}(s)=M^{-1}\Psi(0) \tag{39}$$

with coefficient matrix

$$M=\begin{pmatrix} s+\frac{\gamma_a}{2} & 0 & \mathrm{i}\Omega_{ca}\mathrm{e}^{\mathrm{i}\Phi} & \mathrm{i}\Omega_{da} \\ 0 & s+\frac{\gamma_b}{2} & \mathrm{i}\Omega_{cb} & \mathrm{i}\Omega_{db} \\ \mathrm{i}\Omega_{ca}\mathrm{e}^{-\mathrm{i}\Phi} & \mathrm{i}\Omega_{cb} & s+\frac{\gamma_c}{2}+\mathrm{i}\Delta_c & 0 \\ \mathrm{i}\Omega_{da} & \mathrm{i}\Omega_{db} & 0 & s+\frac{\gamma_d}{2}+\mathrm{i}\Delta_d \end{pmatrix}. \tag{40}$$

The spontaneous emission spectrum of the system $S(\omega_k)=\sum_{i=a,b,c,d}\left|G_k^i(+\infty)\right|^2\rho(\omega_k)$ is obtained from the Fourier transform of $\langle E^-(t+\tau)E^+(t)\rangle_{t\to+\infty}$ [18, 26, 27], with $G_k^i(+\infty)\equiv G_k^i(t)\big|_{t\to+\infty}$ as the long time behavior ($t\to+\infty$) of $G_k^i(t)$. By integrating time t in Eqs. (8)–(11), $G_k^i(+\infty)$ is given by

$$G_k^a(+\infty)=-\mathrm{i}g_k^a\overline{A}\left[i\left(\omega_{ag}-\omega_k\right)\right], \tag{41}$$

$$G_k^b(+\infty)=-\mathrm{i}g_k^b\overline{B}\left[i\left(\omega_{bg}-\omega_k\right)\right], \tag{42}$$

$$G_k^c(+\infty)=-\mathrm{i}g_k^c\overline{\widetilde{C}}\left[\mathrm{i}\left(\omega_{cg}-\Delta_c-\omega_k\right)\right], \tag{43}$$

$$G_k^d(+\infty)=-\mathrm{i}g_k^d\overline{\widetilde{D}}\left[\mathrm{i}\left(\omega_{dg}-\Delta_d-\omega_k\right)\right]. \tag{44}$$

Thus, we find the spontaneous emission spectrum as

$$\begin{aligned} S(\omega_k)=&\frac{\gamma_a}{2\pi}\left|\overline{A}\left[\mathrm{i}\left(\omega_{ag}-\omega_k\right)\right]\right|^2+\frac{\gamma_b}{2\pi}\left|\overline{B}\left[\mathrm{i}\left(\omega_{bg}-\omega_k\right)\right]\right|^2 \\ &+\frac{\gamma_c}{2\pi}\left|\overline{\widetilde{C}}\left[\mathrm{i}\left(\omega_{cg}-\Delta_c-\omega_k\right)\right]\right|^2 \\ &+\frac{\gamma_d}{2\pi}\left|\overline{\widetilde{D}}\left[\mathrm{i}\left(\omega_{dg}-\Delta_d-\omega_k\right)\right]\right|^2 \end{aligned} \tag{45}$$

with $\overline{A}(s)$, $\overline{B}(s)$, $\overline{\widetilde{C}}(s)$, and $\overline{\widetilde{D}}(s)$ given by Eqs. (39) and (40).

In Fig. 4, the spontaneous emission spectra of the system are plotted with different initial conditions: (a) $A(0)=1$ and $B(0)=C(0)=D(0)=0$; (b) $B(0)=1$ and $A(0)=C(0)=D(0)=0$. In Fig. 4 (a), we assume that the system is prepared in level $|a\rangle$ initially, and the black solid curves are for phase $\Phi=\pi/2$ and the red dashed curves for $\Phi=-\pi/2$. When $\Phi=-\pi/2$, as the population can transfer from the level $|a\rangle$ to level $|b\rangle$, so there is a peak around the resonant frequency ω_{bg} in the spontaneous emission spectra. In the meantime, the population can transfer from both the levels $|a\rangle$ and $|b\rangle$ to levels $|c\rangle$ and $|d\rangle$, and the interferences between different population transferring paths suppress the population de-

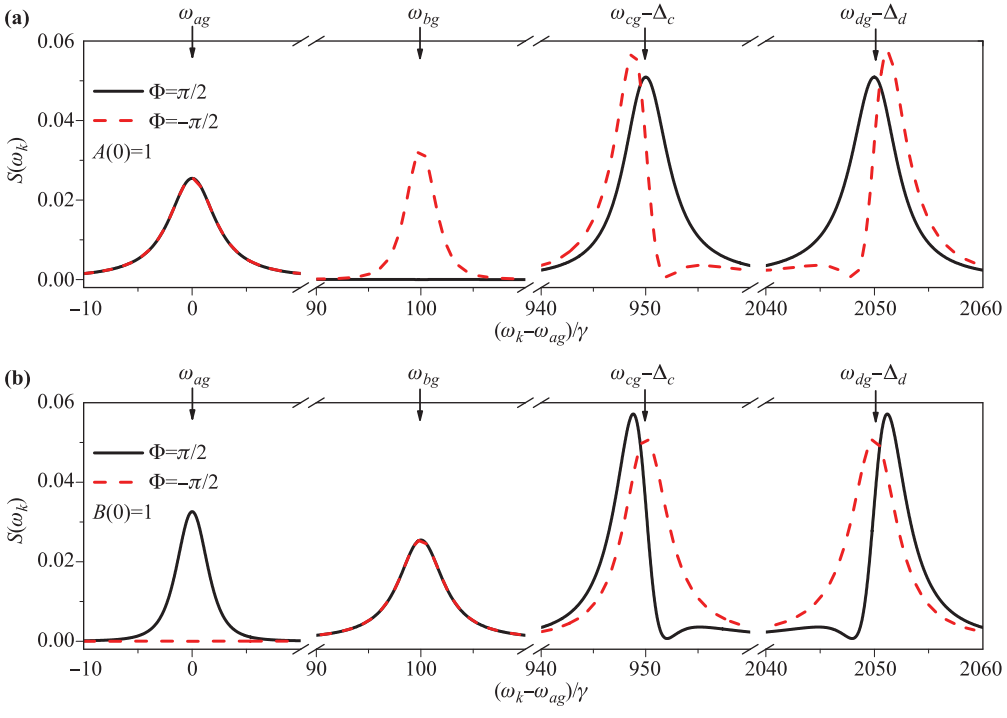

Fig. 4 The spontaneous emission spectrum $S(\omega_k)$ is plotted as a function of the detuning $(\omega_k-\omega_{ag})/\gamma$ for synthetic magnetic flux $\Phi=\pi/2$ (black solid curve) and $\Phi=-\pi/2$ (red dashed curve), with initial conditions $A(0)=1$ and $B(0)=C(0)=D(0)=0$ in (a), and $B(0)=1$ and $A(0)=C(0)=D(0)=0$ in (b). In both (a) and (b), we set $\omega_{bg}-\omega_{ag}=100\gamma$, $\omega_{cg}-\omega_{ag}=1000\gamma$, and $\omega_{dg}-\omega_{ag}=2000\gamma$. The other parameters are the same as in Fig. 2.

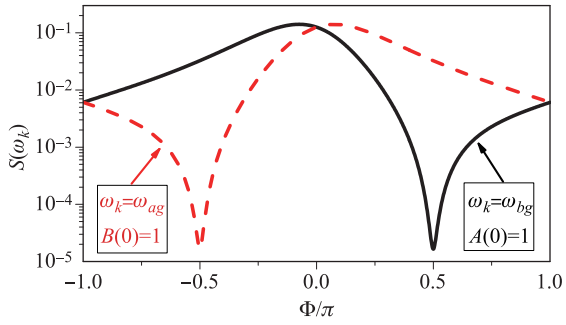

Fig. 5 The spontaneous emission spectrum $S(\omega_k)$ is plotted as a function of the synthetic magnetic flux Φ: (black solid curve) with frequency $\omega_k = \omega_{bg}$ and initial conditions $A(0) = 1$ and $B(0) = C(0) = D(0) = 0$, and (red dashed curve) with frequency $\omega_k = \omega_{ag}$ and initial conditions $B(0) = 1$ and $A(0) = C(0) = D(0) = 0$. The other parameters are the same as in Fig. 4.

cay from levels $|c\rangle$ and $|d\rangle$ [see $|C(t)|^2 = |D(t)|^2$ (blue dashed-dot curve) in Fig. 2(c)] and induce the dips around frequencies $\omega_{cg} - \Delta_c$ and $\omega_{bg} - \Delta_d$. Instead, there is almost no population transferring from the level $|a\rangle$ to level $|b\rangle$ when $\Phi = \pi/2$, so that the peak around the frequency ω_{bg} is eliminated. Meanwhile, the population transfer only from the level $|a\rangle$ to levels $|c\rangle$ and $|d\rangle$, so that the population in levels $|c\rangle$ and $|d\rangle$ decay nearly exponentially [see $|C(t)|^2 = |D(t)|^2$ (blue dashed-dot curve) in Fig. 2(a)] and there are single peaks around the frequencies $\omega_{cg} - \Delta_c$ and $\omega_{bg} - \Delta_d$. In Fig. 4 (b), we assume that the system is prepared in level $|b\rangle$ initially. When $\Phi = \pi/2$, as the population can transfer from the level $|b\rangle$ to level $|a\rangle$, so there is a peak around the resonant frequency ω_{ag} and dips around frequencies $\omega_{cg} - \Delta_c$ and $\omega_{bg} - \Delta_d$ in the spontaneous emission spectra. Instead, there is almost no population transferring from the level $|b\rangle$ to level $|a\rangle$ when $\Phi = -\pi/2$, so that the peak around the frequency ω_{ag} is eliminated and there are single peaks around the frequencies $\omega_{cg} - \Delta_c$ and $\omega_{bg} - \Delta_d$.

In addition, the dependence of the spontaneous emission spectra $S(\omega_k = \omega_{ag})$ and $S(\omega_k = \omega_{bg})$ on the synthetic magnetic flux Φ are shown in Fig. 5, with the system initially prepared in level $|b\rangle$ and $|a\rangle$ respectively. We have $S(\omega_k = \omega_{ag}) > S(\omega_k = \omega_{bg})$ for synthetic magnetic flux $0 < \Phi < \pi$, which corresponds with $T_{ba}(t) < T_{ab}(t)$ in Fig. 3(a); in the contrast, we have $S(\omega_k = \omega_{ag}) < S(\omega_k = \omega_{bg})$ for synthetic magnetic flux $-\pi < \Phi < 0$, conforming to $T_{ba}(t) > T_{ab}(t)$. Thus we can also observe the nonreciprocal transitions by contrasting the difference of the spontaneous emission spectra $S(\omega_k = \omega_{ag})$ and $S(\omega_k = \omega_{bg})$ with the system prepared in level $|b\rangle$ or $|a\rangle$ initially. Moreover, almost all the populations have decayed to the ground states at the time $t = 2/\gamma$, as shown in Figs. 2(a)–(d), so the elimination of spectral lines can be observed within the time scale of $2/\gamma$.

5 Conclusions

Let us now discuss the experimental feasibility of our proposal. Take $^{40}Ca^+$ for example, let us show the corresponding relationship between the energy levels in Fig. 1 and the energy levels of $^{40}Ca^+$: $|a\rangle = |3D_{5/2}\rangle$, $|b\rangle = |3D_{3/2}\rangle$, $|c\rangle = |5P_{3/2}\rangle$, $|d\rangle = |4P_{3/2}\rangle$. First of all, the one-photon dipole transitions $|4P_{3/2}\rangle \leftrightarrow |3D_{5/2}\rangle$, $|4P_{3/2}\rangle \leftrightarrow |3D_{3/2}\rangle$, $|5P_{3/2}\rangle \leftrightarrow |3D_{5/2}\rangle$, and $|5P_{3/2}\rangle \leftrightarrow |3D_{3/2}\rangle$ are allowed, but the one-photon dipole transitions $|5P_{3/2}\rangle \leftrightarrow |4P_{3/2}\rangle$ and $|3D_{5/2}\rangle \leftrightarrow |3D_{3/2}\rangle$ are forbidden, i.e., the cyclic transitions for the four levels can be realized. To avoid the effects of Doppler broadening, the calcium ions should be laser cooled primarily. A single calcium ion can be trapped and laser cooled to 1 mK by Doppler cooling in experiments [31]. According to the experiments with single cold calcium ions [31–34] or few cold calcium ions [35], $|3D_{5/2}\rangle$ and $|3D_{3/2}\rangle$ are metastable levels with lifetimes about 1.2 seconds [31–33, 35], the lifetimes of $|4P_{3/2}\rangle$ is about 6.6 nanoseconds [34, 36], and the lifetimes of $|5P_{3/2}\rangle$ must also be much shorter than 1.2 seconds, i.e., the conditions for adiabatic approximation ($\min\{\gamma_c, \gamma_d\} \gg \max\{\gamma_a, \gamma_b\}$) are satisfied. Hence if four laser fields with appropriate frequencies, strengths, and phases are applied to the $^{40}Ca^+$ system, the proposal is realizable. Moreover, similar energy structures can be found in other singly charged alkaline-earth metals ions, such as $^{88}Sr^+$ [37, 38] and $^{138}Ba^+$ [39–42].

In summary, a theoretically scheme was proposed to realize nonreciprocal transition between two indirectly coupled energy levels in a multi-level atomic system with cyclic four-level configuration. The spontaneous emission spectra of the multi-level system with nonreciprocal transition was also investigated. The nonreciprocal transition results in the elimination of a spectral line in the spontaneous emission spectrum, which can be used to identify the nonreciprocal transition experimentally. As the multi-level atomic system with cyclic four-level configuration can be realized under the rules of electric dipole transitions, the scheme in this paper can be applied for observing nonreciprocal transition in the natural atoms or ions with parity symmetry, which will widely broaden the application sphere of nonreciprocal transition.

Acknowledgements X.-W. X. and H.-Q. S. are supported by the National Natural Science Foundation of China (NSFC) under Grant No. 12064010, the Natural Science Foundation of Hunan Province of China under Grant No. 2021JJ20036, and the Natural Science Foundation of Jiangxi Province of China under Grant No. 20192ACB21002. A.-X. C. is supported by NSFC under Grant No. 11775190.

References

1. R. K. Pathria, Statistical Mechanics, 2nd Ed., Butterworth-Heinemann, Oxford, 1996
2. A. Einstein, On the quantum theory of radiation, *Phys. Z.* 18, 121 (1917)
3. P. Král and M. Shapiro, Cyclic population transfer in quantum systems with broken symmetry, *Phys. Rev. Lett.* 87(18), 183002 (2001)
4. H. Li, V. A. Sautenkov, Y. V. Rostovtsev, G. R. Welch, P. R. Hemmer, and M. O. Scully, Electromagnetically induced transparency controlled by a microwave field, *Phys. Rev. A* 80(2), 023820 (2009)
5. W. Z. Jia and L. F. Wei, Gains without inversion in quantum systems with broken parities, *Phys. Rev. A* 82(1), 013808 (2010)
6. P. Král, I. Thanopulos, M. Shapiro, and D. Cohen, Two-step Enantio-selective optical switch, *Phys. Rev. Lett.* 90(3), 033001 (2003)
7. Y. Li, C. Bruder, and C. P. Sun, Generalized Stern–Gerlach effect for chiral molecules, *Phys. Rev. Lett.* 99(13), 130403 (2007)
8. Y. X. Liu, J. Q. You, L. F. Wei, C. P. Sun, and F. Nori, Optical selection rules and phase-dependent adiabatic state control in a superconducting quantum circuit, *Phys. Rev. Lett.* 95(8), 087001 (2005)
9. J. E. Mooij, T. P. Orlando, L. Levitov, L. Tian, C. H. van der Wal, and S. Lloyd, Josephson persistent-current qubit, *Science* 285(5430), 1036 (1999)
10. L. Zhou, L. P. Yang, Y. Li, and C. P. Sun, Quantum routing of single photons with a cyclic three-level system, *Phys. Rev. Lett.* 111(10), 103604 (2013)
11. Y. X. Liu, H. C. Sun, Z. H. Peng, A. Miranowicz, J. S. Tsai, and F. Nori, Controllable microwave three-wave mixing via a single three-level superconducting quantum circuit, *Sci. Rep.* 4(1), 7289 (2015)
12. Y. J. Zhao, J. H. Ding, Z. H. Peng, and Y. X. Liu, Realization of microwave amplification, attenuation, and frequency conversion using a single three-level superconducting quantum circuit, *Phys. Rev. A* 95(4), 043806 (2017)
13. Z. H. Wang, C. P. Sun, and Y. Li, Microwave degenerate parametric down-conversion with a single cyclic three-level system in a circuit-QED setup, *Phys. Rev. A* 91(4), 043801 (2015)
14. A. Barfuss, J. Kölbl, L. Thiel, J. Teissier, M. Kasperczyk, and P. Maletinsky, Phase-controlled coherent dynamics of a single spin under closed-contour interaction, *Nat. Phys.* 14(11), 1087 (2018)
15. X. W. Xu, Y. J. Zhao, H. Wang, A. X. Chen, and Y. X. Liu, Nonreciprocal transition between two nondegenerate energy levels, *Photon. Res.* 9(5), 879 (2021)
16. J. Zhang, B. Peng, I. M. C. K. Özdemir, Y. X. Liu, H. Jing, X. Y. Lü, Y. L. Liu, L. Yang, and F. Nori, Giant nonlinearity via breaking parity-time symmetry: A route to low-threshold phonon diodes, *Phys. Rev. B* 92(11), 115407 (2015)
17. Y. Jiang, S. Maayani, T. Carmon, F. Nori, and H. Jing, Nonreciprocal phonon laser, *Phys. Rev. Appl.* 10(6), 064037 (2018)
18. X. W. Xu, C. Ye, Y. Li, and A. X. Chen, Enantiomeric-excess determination based on nonreciprocal-transition-induced spectral-line elimination, *Phys. Rev. A* 102(3), 033727 (2020)
19. N. A. Ansari, J. Gea-Banacloche, and M. S. Zubairy, Phase-sensitive amplification in a three-level atomic system, *Phys. Rev. A* 41(9), 5179 (1990)
20. C. A. Blockley and D. F. Walls, Intensity fluctuations in a frequency down-conversion process with three-level atoms, *Phys. Rev. A* 43(9), 5049 (1991)
21. H. Ritsch, P. Domokos, F. Brennecke, and T. Esslinger, Cold atoms in cavity-generated dynamical optical potentials, *Rev. Mod. Phys.* 85(2), 553 (2013)
22. M. Brownnutt, M. Kumph, P. Rabl, and R. Blatt, Ion-trap measurements of electric-field noise near surfaces, *Rev. Mod. Phys.* 87(4), 1419 (2015)
23. M. Tomza, K. Jachymski, R. Gerritsma, A. Negretti, T. Calarco, Z. Idziaszek, and P. S. Julienne, Cold hybrid ion-atom systems, *Rev. Mod. Phys.* 91(3), 035001 (2019)
24. P. Lodahl, S. Mahmoodian, S. Stobbe, A. Rauschenbeutel, P. Schneeweiss, J. Volz, H. Pichler, and P. Zoller, Chiral quantum optics, *Nature* 541(7638), 473 (2017)
25. T. Ozawa, H. M. Price, A. Amo, N. Goldman, M. Hafezi, L. Lu, M. C. Rechtsman, D. Schuster, J. Simon, O. Zilberberg, and I. Carusotto, Topological photonics, *Rev. Mod. Phys.* 91(1), 015006 (2019)
26. S. Y. Zhu, R. C. F. Chan, and C. P. Lee, Spontaneous emission from a three-level atom, *Phys. Rev. A* 52(1), 710 (1995)
27. S. Y. Zhu and M. O. Scully, Spectral line elimination and spontaneous emission cancellation via quantum interference, *Phys. Rev. Lett.* 76(3), 388 (1996)
28. V. Weisskopf and E. Wigner, Berechnung der natürlichen linienbreite auf grund der diracschen lichttheorie, *Z. Phys.* 63(1–2), 54 (1930)
29. M. O. Scully and M. S. Zubairy, Quantum Optics, Cambridge University Press, Cambridge, UK, 1997
30. H. F. Song, Y. B. Tang, S. L. Chen, L. J. Du, Y. Huang, H. Guan, and K. L. Gao, Combined experimental and theoretical probe of the branching fractions of the $4P_{3/2}$ state in $^{40}Ca^{+}$, *Phys. Rev. A* 100(5), 052505 (2019)
31. P. A. Barton, C. J. S. Donald, D. M. Lucas, D. A. Stevens, A. M. Steane, and D. N. Stacey, Measurement of the lifetime of the $3d^2D_{5/2}$ state in $^{40}Ca^{+}$, *Phys. Rev. A* 62(3), 032503 (2000)
32. A. Kreuter, C. Becher, G. P. T. Lancaster, A. B. Mundt, C. Russo, H. Häffner, C. Roos, W. Hänsel, F. Schmidt-Kaler, R. Blatt, and M. S. Safronova, Experimental and theoretical study of the $3d^2D$-level lifetimes of $^{40}Ca^{+}$, *Phys. Rev. A* 71(3), 032504 (2005)
33. H. Shao, Y. Huang, H. Guan, Y. Qian, and K. Gao, Precision measurement of the $3d^2D_{3/2}$-state lifetime in a single trapped $^{40}Ca^{+}$, *Phys. Rev. A* 94(4), 042507 (2016)

34. Z. Meir, M. Sinhal, M. S. Safronova, and S. Willitsch, Combining experiments and relativistic theory for establishing accurate radiative quantities in atoms: The lifetime of the $2P_{3/2}$ state in $^{40}Ca^{+}$, *Phys. Rev. A* 101(1), 012509 (2020)

35. P. Staanum, I. S. Jensen, R. G. Martinussen, D. Voigt, and M. Drewsen, Lifetime measurement of the metastable $3d^2D_{5/2}$ state in the $^{40}Ca^{+}$ ion using the shelving technique on a few-ion string, *Phys. Rev. A* 69(3), 032503 (2004)

36. J. Jin and D. A. Church, Precision lifetimes for the Ca^{+} $4p^2P$ levels: Experiment challenges theory at the 1% level, *Phys. Rev. Lett.* 70(21), 3213 (1993)

37. S. Mannervik, J. Lidberg, L. O. Norlin, P. Royen, A. Schmitt, W. Shi, and X. Tordoir, Lifetime measurement of the metastable $4d^2D_{3/2}$ level in Sr^{+} by optical pumping of a stored ion beam, *Phys. Rev. Lett.* 83(4), 698 (1999)

38. V. Letchumanan, M. A. Wilson, P. Gill, and A. G. Sinclair, Lifetime measurement of the metastable $4d^2D_{5/2}$ state in $^{88}Sr^{+}$ using a single trapped ion, *Phys. Rev. A* 72(1), 012509 (2005)

39. N. Yu, W. Nagourney, and H. Dehmelt, Radiative lifetime measurement of the Ba^{+} metastable $D_{3/2}$ state, *Phys. Rev. Lett.* 78(26), 4898 (1997)

40. E. A. Dijck, A. Mohanty, N. Valappol, M. N. N. Portela, L. Willmann, and K. Jungmann, Lifetime of the $5d^2D_{5/2}$ level of $^{138}Ba^{+}$ from quantum jumps with single and multiple Ba^{+} ions, *Phys. Rev. A* 97(3), 032508 (2018)

41. J. Gurell, E. Biémont, K. Blagoev, V. Fivet, P. Lundin, S. Mannervik, L. O. Norlin, P. Quinet, D. Rostohar, P. Royen, and P. Schef, Laser-probing measurements and calculations of lifetimes of the $5d^2D_{3/2}$ and 5 $d^2D_{5/2}$ metastable levels in Ba II, *Phys. Rev. A* 75(5), 052506 (2007)

42. M. D. Havey, L. C. Balling, and J. J. Wright, Direct measurements of Ba^{+} excited-state lifetimes, *Phys. Rev. A* 15(6), 2332 (1977)